Evaluation of flow-rate dynamics in the simultaneous photocatalytic treatment of multichlorinated substituted phenols in continuous-flow systems

Z. Khuzwayo, E.M.N Chirwa

Department of Chemical Engineering, Water Utilisation Division, University of Pretoria, Pretoria, 0002 South Africa. Tel.: +27793797619, E-mail: zack.khuzwayo@up.ac.za.

Abstract

The project investigated the simultaneous degradation of chlorophenols dissolved aqueous systems. The photocatalysis advanced oxidation process was the technology applied to achieve treatment. Chemical behavioural tracking was performed using the chloride dehalogenation sequence dynamics. The study recorded reductive dehalogenation chemical transformation kinetics of multi-substituted chlorinated phenolics in continuous flow reactor systems. This was performed by manipulation of liquid flow-rates in the photocatalytic oxidations process using suspended and immobilised catalyst applications. A modified Langmuir-Hinshelwood kinetic model was proposed that explained the oxidation transformational behaviour of the dehalogenation process derived intermediates. Complementary photocatalytic performance matrices were established for each flow regime, model parameters were calculated and estimated for behavioural profiles of all compounds under scrutiny.

Keywords: Photocatalysis, chlorophenols, continuous-flow reactors, water treatment

Introduction

Improved chemical technology worldwide has been coupled with increased chemical pollutants in the environment (Chen et al., 2000). A concerning factor is that the chemical pollutants are not only increasing in diversity, the concentration levels in the environment are increasing yearly. Additionally, current water treatment technologies are ineffective at treating or removing these emerging pollutants. One of the more effective technological disciplines in dealing with emerging pollutants is photocatalysis. Photocatalysis is non-selective and capable of completely mineralizing most organic chemical species (Angelo et al., 2013; Demeestere et al., 2007; Carp et al., 2004). Though photocatalysis has proven a useful technology in the mineralization of organic pollutants (Malato et al., 2009; Lathasree et al., 2004; Davis and Huang, 1990), the next stage in its theoretical implementation would be the understanding of the technology's induced transformation behaviour of different classes of compounds. Though the photocatalytic mechanism and the oxidation reactions associated with it are adequately understood, the processes of chemical transformations and the mechanisms preferred are unclear. Treatment processes require consideration of the reaction pathways and derivative reaction schemes followed to optimize the overall performance.

In the photocatalytic mechanism, surface bound electrons are ejected from the semiconductor particle surface (valence band) to a higher energy band edge (conduction band). The elevation of electrons from the valence band to the conduction band causes charge separation that is followed by

the scavenging of electrons and pairing holes by surface adsorbed chemical groups. This facilitates redox processes that include proton reduction, oxygen reduction, direct oxidation, water splitting, current doubling, reductive dehalogenation, and hydroxyl radical ion oxidation. The hydroxyl radical attack is the mechanism that is predominantly credited for the photocatalytic principle, and in many cases the effect of other generated pathways in negated. One such pathway is that of reductive dehalogenation, this study approach seeks to confirm and evaluated the photocatalytic performance and transformation behaviour of the dehalogenation process. That which pertains significantly to this approach is the theoretical foundations of the photocatalytic behavioural principle in application to different chemical groups and the lack of unison in scientific literature. The complexity of heterogeneous advanced oxidation is a challenging one in that many steps and reaction mechanism may be operating simultaneously (Yasmina et al., 2014; Pozzo et al., 1997). A simple example to elucidate the complexity of the process is how kinetic separation of the photolytic process is not possible from that of photocatalysis as these processes happen interdependently (or at least for semiconductor catalyst involvement). Chemical transformations of most photocatalytic systems and their performances are mostly speculative. Established and constructed mathematical models only aid in unravelling more scientific mystery. The proposed approach puts impetus on the chemical kinetic variability of the transformation potential of related species within the photocatalytic process. This study will attempt to determine the kinetic trail and the dehalogenation reaction routes undertaken in the oxidation process towards mineralisation.

Many related and unrelated classes of chemical groups are found dissolved in aqueous matrices, but the typical approach is to identify markers that can represent and be extrapolated into deterministic behaviour (Nugraha and Fatimah, 2013; Oller et al., 2011). This might be plausible in simple applications of the advance oxidation process such as photolysis, where the destruction of the relevant compounds is a function of structural and functional group complexity in combination to light source properties. Photocatalysis though a highly promising technology will need to overcome its shortfalls for effective applications, but more importantly its theoretical basis in performance needs to be well understood as very few standard models exist that can be applied from one unique setup to another (Pera-Titus et al., 2004; Pelentridou et al., 2004). For photocatalysis to realize its true potential the system will need to function in a continuous flow manner, similarly to current treatment process function in treatment facilities. The ultimate objective in the chemical treatment photocatalytic performance agenda is to reach standardisation; this is seldom achieved in most application, even those that follow simpler reaction mechanisms. Not much research has been conducted on the continuous flow nature of photocatalytic application, as a significant amount of application is still in static systems. Practical limitations to photocatalysis are that related to the catalyst (semiconductors) recovery when dispensed in slurry forms, and the inabilities to maximize particle efficiency. This study will attempt to model transformative behaviour of multichlorinated substituted phenols in simultaneous pollutant matrices using kinetic and simulated statistical models.

Experimental

Materials

4-chlorophenol (MCP) 99% purity, 2.4-dichlorophenol (DCP) 99%, 2.4.6-trichlorophenol (TCP) 98%, pentachlorophenol (PCP) 97%, and anatase 99.7% titanium dioxide (TiO_2) were purchased from Sigma-Aldrich Logistik GmbH (Schnelldorf, Germany). Phenol and GC grade methanol were purchased from Merk (South Africa). Ultra-pure (UP) water was dispensed by the Millipore Direct Q3 with pump instrument. Reference standard were purchased from PerkinElmer (South Africa division).

Instrumental analysis

Polychlorinated phenolics and derivative products were analysed using a gas chromatography (GC) system comprising of a clarus 600 GC, clarus 600T mass spectrometer (MS), attached to a turbomatrix 40 trap headspace sampler (PerkinElmer, South Africa division). The chemical separation component was the Elite 5MS GC system capillary column (30 m, 250 µm) from PerkinElmer. Helium (He) carrier gas of 99.999% purity and applied at a flow rate of 1 mL min^{-1}. MS interface comprised of an Electron Ioniser (EI) and a high performance mass analyser.

Data processing, kinetic and modelling

Sigmaplot 11 scientific data analysis graphics computation software was used for data processing and statistical analysis. Aquasim 2.0 computer program for the identification and simulation of aquatic systems was used to simulate and model the photocatalytic oxidation profiles, and parameter estimations.

Series reactors configuration

The setup was installed in a temperature regulated walk-in reactor room that is wall-connected to a cold room of 4 °C set temperature. The wall connection has port-openings that allow transfer of cooled air, driven by a pressure-vacuum system. The reactor system was configured on a wall-bench structure. Four 400 mL transparent glass reactors vessels were mounted on stands side-by-side (30 cm apart). Each vessel had oxygen (O_2) of 99 % purity delivery tube connected to a regulator, and connected to a longitudinal fizzle nozzle. In between the four vessels were 3 quartz glass sleeves mounted equidistant from each vessel. Encased in the quartz sleeves were long-arc 400 Watts (Philips HOK 4/120 SE) medium pressure lamps, details in Table 1. The two reactor vessels on the ends received radiation source from single lamps, while the two middle mounted reactors were exposed to radiation sources from both directions. Five independent electrostatic pumps were employed connected to simulate natural flow. Figure 1 shows the reactor schematic diagrams.

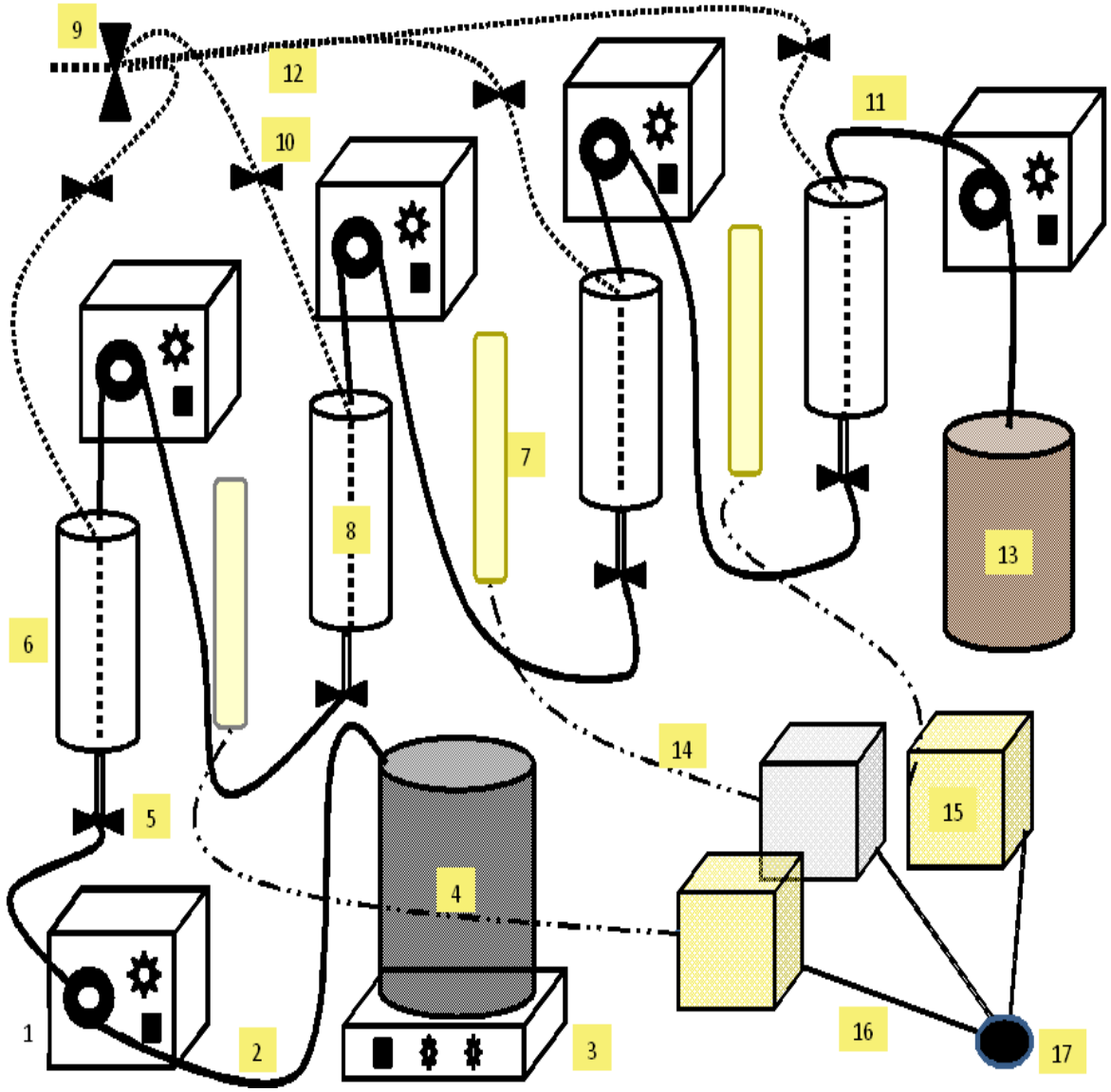

1. Electrostatic pumps
2. Precision tubing (Black)
3. Magnetic stirrer
4. Source Reservoir (light blocked)
5. Regulated source inlet
6. Reactor vessels
7. UV Lamps
8. Oxygen delivery fizzle tube
9. Main source oxygen regulator
10. Oxygen flow meters
11. Outlet tubes
12. Oxygen delivery tubing (translucent)
13. Treated solution reservoir
14. Lamp connection cables
15. Power ballasts
16. Power cable
17. Power source
18. Unseen connection cabling

Figure 1 Detailed schematic representation of the continuous flow reactors assembled in series

Table 1 Lamp properties used to configure the reactors system

Lamp	Length (mm)	Width (mm)	Wattage	Radiation Details (W) UVA	UVB	UVC	Voltage (V)
HOK4/120	100	16	400	31	32	52	120

Immobilisation of photocatalyst

Recycled transparent glass (Schott Duran) of 2 000 g mass was sized between 8 mm and 20 mm in dimensions, rinsed with tap water and dried in heating oven at 100 ◦C for 2 hours. 2 g of anatase titanium dioxide powder was mixed in 1 L of ultra-pure water, magnetically stirred at 200 rpm for 2 hours. The glass was completely submerged in the think catalyst slurry mixture. It was then drip-hung for less than 30 minutes to allow thin coat development and transferred to a high-temperature heating plate. The plate was placed in a furnace (Thermo-power furnace) oven at 500 ◦C for 48 hours. The next step was cooling to room temperature and water submerging for 30 minutes then dried in an incubator oven at 60 ◦C for 2 hours. A finely thin resistant layer of titanium dioxide (Figure 2) coating was established. Random glass pieces were tested for transparency using spectroscopy (WPA Lightwave II, Labotech), the recorded average transmittance percentage was 53 ± 4.4 (n = 10) in the wavelength range of 270 to 330 nm. The goal was to establish a think enough spatial coated catalyst film to facilitate adsorption while allowing adequate incidence light to pass-through at areas perpendicular to the glass surface. The glass packing process into the reactor vessel was neither specific nor pattern-structured, glass units were delicately filled into each vessel.

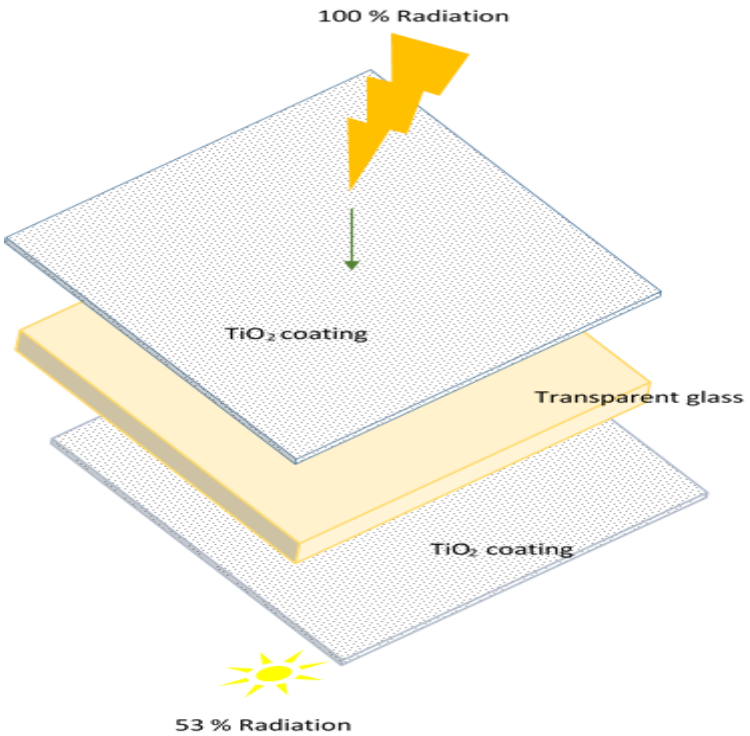

Figure 2 Schematic representation of the immobilised TiO_2 on glass and radiation transfer through it

Experimental procedure

A source solution reservoir (label 4 in Figure 1) was prepared in a 5 L amber flask by spiking ultra-pure water with chlorophenol reagents to attempted concentrations of 10 mg L^{-1}. The suspended catalyst sets were dispensed with pure anatase particles of a mass equivalent to 30 mg L^{-1}, the reservoir solution was sonicated for a period of 15 minutes before transfer onto a magnetic stirrer that was set at 200 rpm. The immobilised catalyst sets reservoir solutions were prepared similarly without the application of the catalyst step. The solution flow-rates were set by manual measurements of displaced volume and the time taken, this was repeated many times to verify the set dials on the solution feed driving pump (Table 2). The catalyst immobilised glass network packed vessels were prepared with a detention time consideration, an average of 170 mL glass material displacement volume was prepared in all four vessels. The detention periods calculated were strictly the measurements of the vessel solution volumes, not including the solution occupied in the connecting tubing. Pure oxygen was delivered through nozzle outlets with set flow-rates of 20 mL min^{-1} from a central source, the gas was turned on before solution delivery for optimum uninterrupted bubbling, and the 20 mL min^{-1} flow also provided adequate longitudinal mixing. After time zero sampling, the lamps were turned on immediately after the driving system was initiated. A minimum of three sampling intervals were identified in each detention period for all vessels (the longer detention periods allowed for more sampling points), sampling took place at approximately the same vessels location for consistency.

Table 2 Continuous-flow reactor variables and properties

Catalyst	RV	PRV	Q_i	D_t	Min # Periods
Suspended	400	-	9; 15; 30	45; 27; 13	8
Immobilised	400	230 ± 5	9; 15; 28	26; 15; 8	8

Reactor volume mL (RV), packed reactor volume mL (PRV), Detention time min^{-1} (D_t), Flow rate (Q_i) mL min^{-1}. Time (mins)

Each vessel was sampled n-times in each detention period for a minimum of 8 cycles. All cycles per vessels of the same sampling interval were used to calculate the average concentration e.g. Vessel 1 at time 5 minutes was measured 8-times or more, same for vessel-n at time-n. 500 µg L^{-1} solution samples were removed for each measurement, all samples were centrifuged at 5000 rpm for 10 minutes. 2 µL of the supernatant was analysed using the GCMS.

Theoretical model

Kinetic model

The Langmuir–Hinshelwood (L-H) model is the most commonly used kinetic expression to explain the kinetics of the heterogeneous catalytic processes (Kumar et al., 2008). The expression has been successfully used for heterogeneous photocatalytic degradation to determine the relationship between the initial degradation rate and the initial concentration of the organic substrate (Saien and Khezrianjoo, 2008). The L-H expression assigned for heterogeneous photocatalytic behaviour takes the form of Eq.1, where *r* is the rate of the reaction, *k* is the rate of surface reaction constant, *K* is the Langmuir-Hinshelwood semiconductor adsorption equilibrium constant, and *C* is the concentration of the analyte.

$$r = \frac{k K C}{1 + K C} \qquad (1)$$

L-H kinetic adsorption equilibrium isotherms were calculated in a complimentary study by Khuzwayo and Chirwa (2015) on the same chemical species using Eq.2 where Q_e is the adsorbed chemical concentration per weight of adsorbent at equilibrium (mg g^{-1}), C_e is the final equilibrium solution concentration (mg L^{-1}), K_L is the free energy Langmuir adsorption constant (mg L^{-1}), and Q_m is the maximum adsorption capacity (mg g^{-1}).

$$Q_e = \frac{Q_m K_L C_e}{1 + K_L C_e} \qquad (2)$$

The Langmuir-Hinshelwood kinetics, though plausible at the determination of rate of reaction profiles and calculation of parameters through linearisation of Eq.2, it cannot account for fractional chemical transformation profiles and derived intermediates when fluctuating and compounding chemical dynamics are recorded. Though the heterogeneous semiconductor surface reactions may determine the oxidation mechanism of each individual compound in a matrix, the transformational accumulative effect of related chemical derivatives may deviate from the L-H determined profiles.

Figure 3 shows the profile representation of the photocatalytic degradation of one of the chlorophenols in the sequence of four reactors. The graphical profiles of the reactors are separated into four rectangular boxes that are differentiated by bold, dotted, short and long dotted lines. The transformational behaviour of each profile in Figure 3 appears different from one to the next. These behaviour profiles do not strictly adhere to the expected L-H kinetics, in fact the profile fragments were found to encompass multiple processes that outline the predominant transformational processes at different stages. Though it is understood that the prevalent oxidation mechanism follows Langmuir-Hinshelwood principles, the detected concentrations with the exception of the highest level substituted chlorophenol (PCP) registered modified kinetics. The behaviour of the profiles showed involvement of exponential population dynamics. The dotted line of reactor two recorded an increasing form of exponential decrease in concentration and the same but to a lesser extent in the fourth reactor, other data not depicted in Figure 3 recorded decreasing forms of

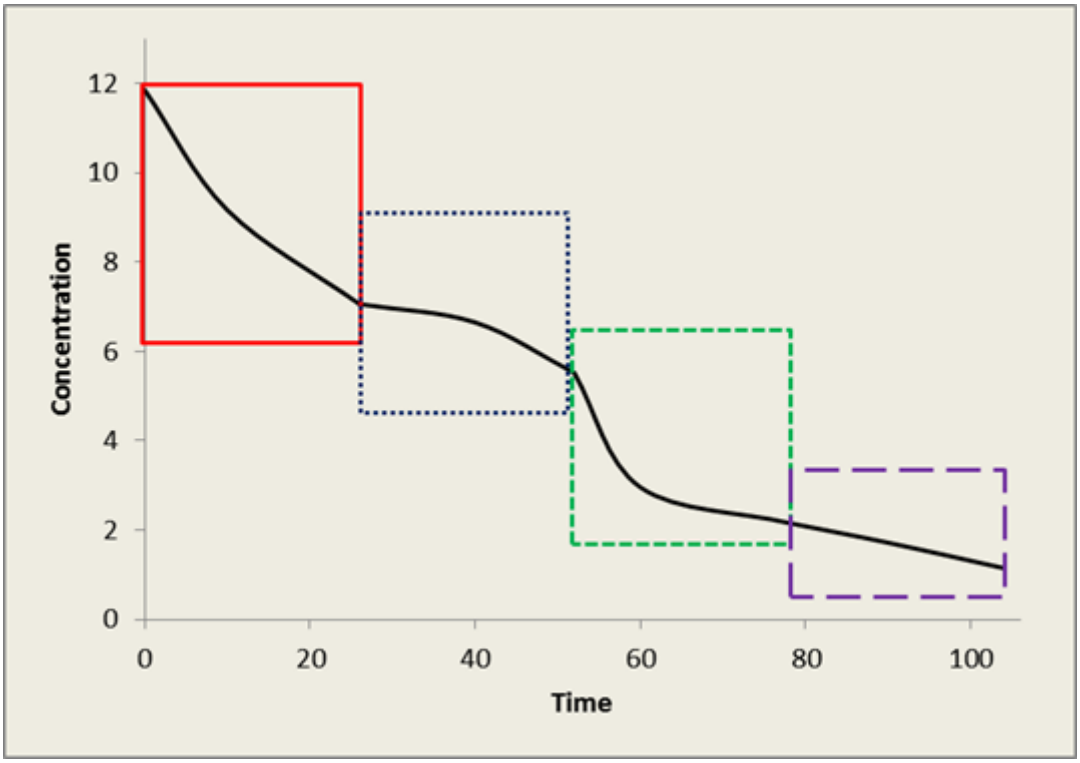

Figure 3 Depiction of the time course profile transformations in continuous-flow reactors

exponential increase. An appropriate model would encompass the chemical population behaviour dynamics and the Langmuir-Hinshelwood expression. The Langmuir-Hinshelwood expression needed to incorporate chemical compounds concentration growth and decay expressions in order to model the most probable chemical reactions and profile behaviours. The incremental changes in compound concentrations that deviated from the Langmuir-Hinshelwood kinetics were a function of the oxidised higher-level substituted chlorinated phenols transformation and the rate constant at which the conversion to the lower-level substituted chlorinated phenol took place. Eq.3 shows the L-H and populations dynamics coupled expression.

$$\frac{dC_n}{dt} = \frac{k_n.K_n.C_n}{1+(K_n.C_n)} + \begin{matrix} R_n.exp^{(k_{2}n.t)} \\ or \\ R_n.(1\text{-}exp^{(k_{2}n.t)}) \end{matrix} \qquad (3)$$

Where the subscript letter (*n*) represents each chlorophenol compound in the expression. An independent parameter R_n is introduced to the expression, which represents the fraction of the higher-level chloride substituted phenol converted to the subsequent formation of derived intermediate analyte of interest, and k_{2n} represents the rate of formation of the derived lower level specie in question. The model proposed renders the degradation rate constants and the Langmuir adsorption constants estimations as a function of the photocatalytic process, while the additional incorporated growth model parameters will behave as functions of exponential variations of the recorded and simulated data profiles. The transformation resultant accumulative behaviour of the lower level chlorophenols could not be bracketed with the concentration of each species given that

profile dependent calculations were required, and in addition, all four reactors had different initial and final concentrations, and the readings for repeat cycles were expectedly not identical. This resulted in statistical variants that were represented as standard deviations for the same detentions period sampling intervals in all respective cycles of each reactor vessels.

Model limits

The Langmuir adsorption estimated parameters of continuous-flow systems were extrapolated from batch adsorption isotherm determinations and the Langmuir-Hinshelwood model respectively, and are expected to deviate from those of batch systems. The calculated estimates and associated deviations with respect to the catalyst Langmuir adsorption constants from the batch reactor values cannot be represented as a function of concentration in combination with the oxidation rate constant, as this would compound deviation uncertainties resulting from batch system values and errors associated with values calculated from continuous-flow reactor determinations. Appropriation limits to the model would need to be strictly defined so as not to undermine the primary oxidation role of the L-H principles from the subsequent fractional formations.

The modelling software was manually used to determine and verify primary parameters limits (k and K), this was performed by hold all parameters at given localised values except for the parameter in question, before the expression optimisation process was initiated. The Langmuir adsorption constant starting value calculated in batch systems was incrementally shifted away from the given reference, this was done until a point was reached when any numerical modification beyond that point made no impression on the profile. This was performed positively and negatively to each end of the reference value and an error range was calculated and included in the model limit. The rate degradation constant limits determinations were a bit more intricate to define since the weight of it contribution could numerically be direct against the secondary functions (R_n and k_{2n}) and inverse and still a plausible profile could be maintained. The approach that put appropriate weight on the primary function was to determine and set the rate constants at its most efficient according to the profile inclination and through manipulation of the secondary functions, the highest and lowest values were set that did not throw the model out of range.

The secondary functions were very low fractional contributions, one of these parameters in most cases was directly affected by the other, so minor shifts in values from those in compliment to the rate constant settings would easily throw the model off, so limits were set within the range of values that would maintain the integrity of the model.

Results

Configured reactor system analysis

The reactor system applied in this study conforms neither to an ideal complete-mix nor an absolute open plug-flow, it however draws characteristics from both. Complete-mix reactors are assumed to achieve instantaneous mixing that is uniform throughout the reactor. Without a designated mixing mechanism in the current system, mixing is facilitated by longitudinal liquid displacement and rigorous gas bubbling. In conventional plug-flow systems, fluids flow through the reactor compartment with little or absent longitudinal mixing in lateral designed reactors, and with little or absent lateral mixing in longitudinal designed reactors. The designed setup aligns more to the longitudinal format, so lateral mixing is limited to gas induced turbulence. The oxygen fizzle tube had outlet pores longitudinally pierced below maximum solution height, this is assumed to deliver significant lateral dispersion. The series nature of the reactor setup corresponds to hydraulic flow regimes of plug flow reactors, this is idealised when the system consists of infinite number of reactors (Metcalf and Eddy, 2003). The reactor configuration allows for performance analysis of irradiation intensity applications. The boundary-mounted vessels are exposed to single-sided lamp irradiation while the inner-mounted vessels are exposed to double-sided irradiation. Comparative performance analysis is intrigued by each chlorophenols transformation with regards to its independent degradation and conversion, coupled with the generation and accumulation of less substituted derived chlorophenols under scrutiny. The rate of each process will differ from one reactor to the next and this will be driven by the irradiation intensity variable, which will be facilitated by the offsetting of degradation versus formation processes of each chlorophenol taking into account initial concentrations and the propensity of each compound's degradation in relation to other chlorophenols.

Photocatalytic oxidation of chlorophenols in suspended catalyst

Photocatalytic degradation in continuous-flow reactors of the type under study is mostly dependent on resident detention time and exposure to the transforming source. The manipulation of liquid flow-rates is the method used to interrogate the process efficiency in the photocatalytic treatment of polychlorinated organic compounds. The complexity of the photooxidation process though effective on the surface in the treatment of target pollutant species, the multitude of organics and their nature as found in conventional industrial discharges and wastewater can render the process ineffective from a mineralisation point of view. To effectively determine the efficiency of treatment in natural water flow systems and the impact of flow control conditions, flow-rate performance matrices were established from modelled estimations of the transformational behaviour of each of the five compounds identified in the study. The compound performance matrices were directly extrapolated from modelled data graphical plots to easier elucidate the information presented. Kinetic parameter estimations of the proposed model are represents in Table 3. Figure 4 is the photocatalytic performance matrix for the simultaneous degradation of the four chlorophenols and phenol at the flow rate of 9 mL min^{-1}, which is the slowest flow rate setting used for the interrogation of degradation kinetics across the four-reactor treatment system. What the performance matrices will show is that the photocatalytic degradation mechanism is not only

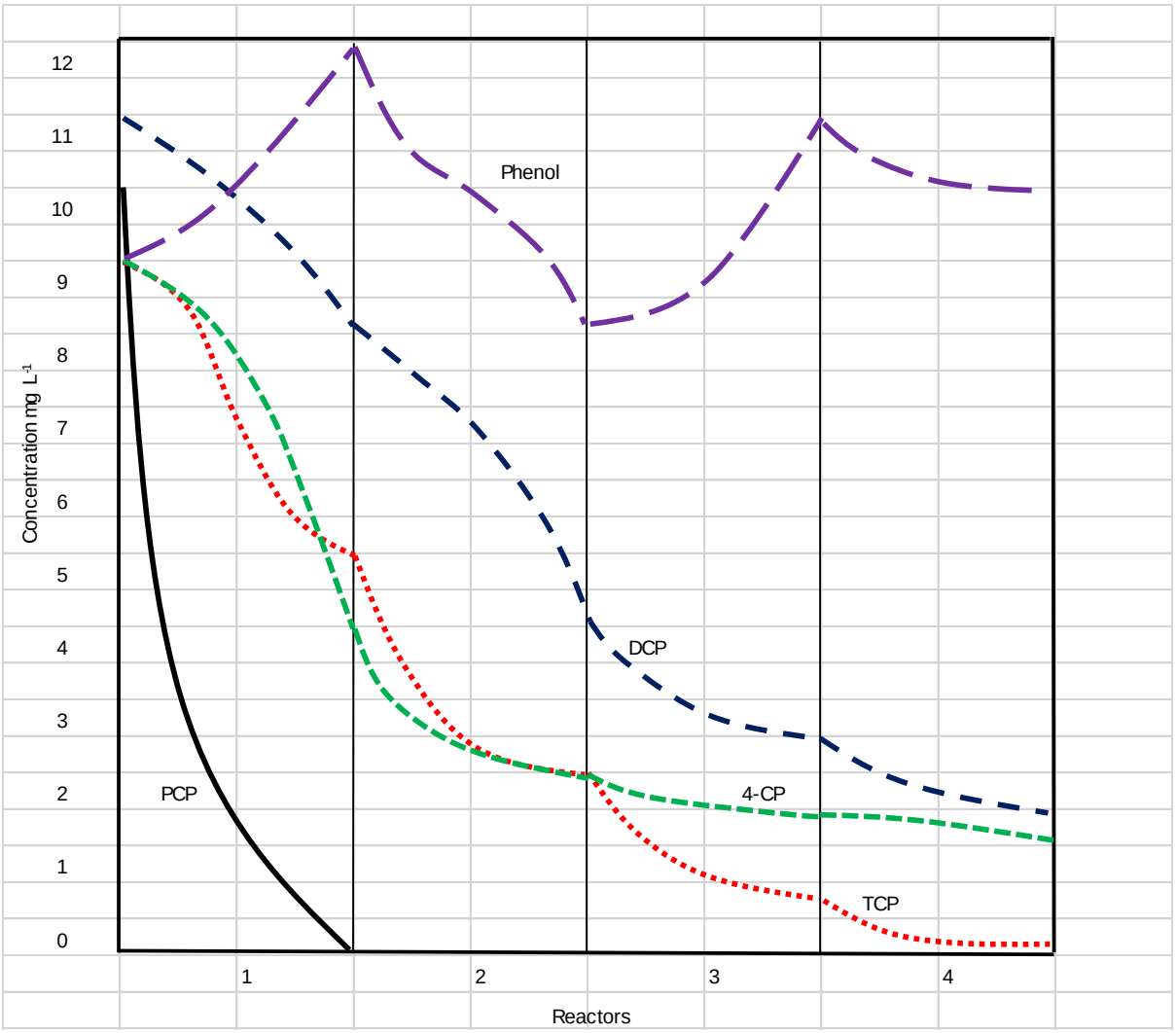

Figure 4 Performance matrix profiles of the photocatalytic degradation of chlorophenols and phenol in continuous-flow reactors configured in series under suspended catalyst conditions. [TiO_2] 30 mg L^{-1}; Oxygen flow – 20 mL min^{-1}; Flow rate – 9 mL min^{-1}; [Analytes] ≈ 10 mg L^{-1}.

confined to the hydroxyl attack pathways at the surface of the valence band edge, many other reaction schemes are in process. The reaction scheme that explains the transformation behaviour of the profiles exhibited is the dehalogenation of multi-substituted chlorinated phenols that leads to the formation of lesser substituted species. It is important to note that all performance matrices and supporting data shows that the higher chloride-substituted phenol compounds disappear at a faster rate than lower-substituted compounds. The degradation sequence is in agreement with a paper published by IPCBEE (2015) on batch systems. The 9 mL min^{-1} performance matrix shows that PCP was completely degraded in the first reactor of a maximum detection period of 45 minutes.

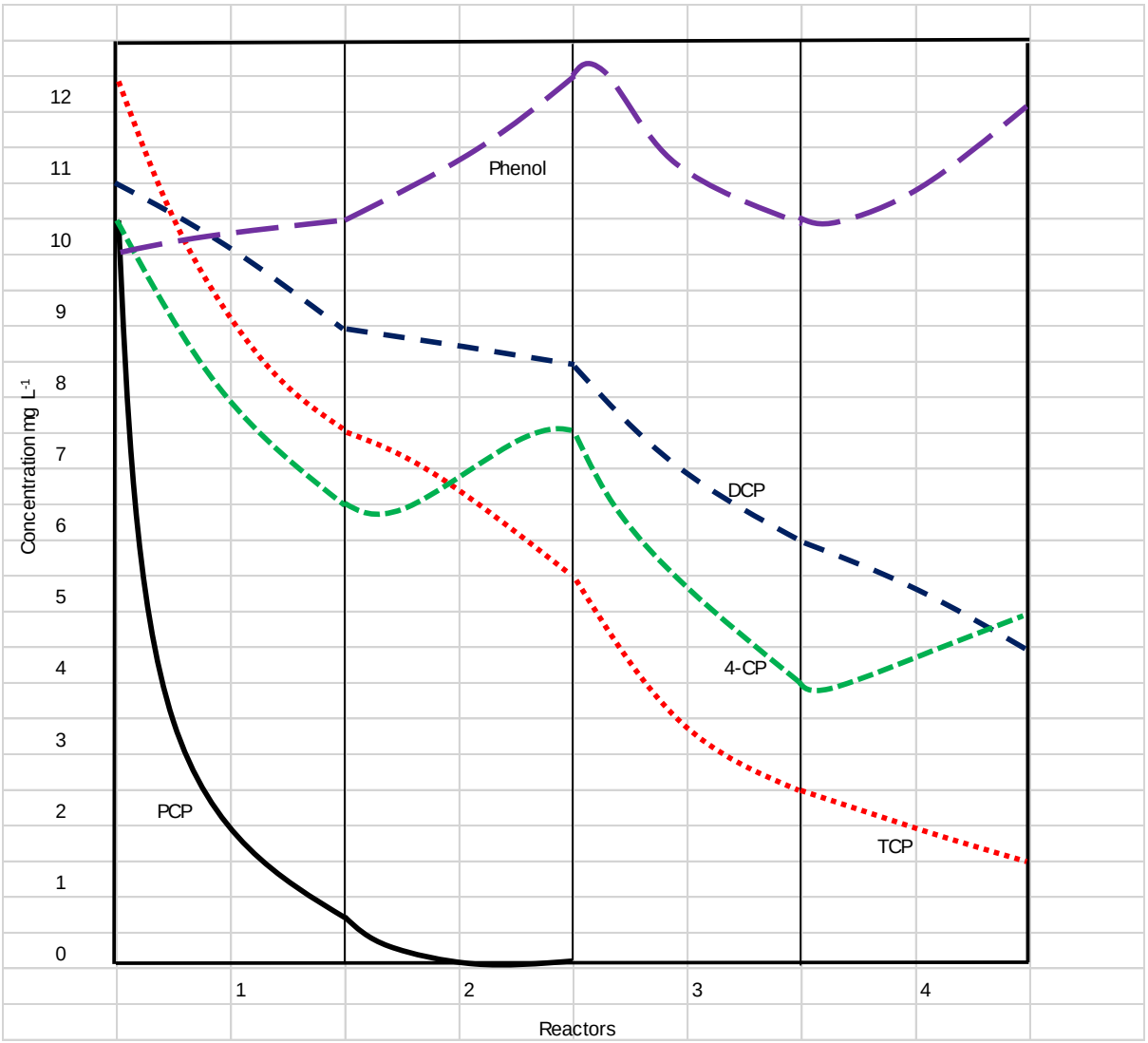

Figure 5 Performance matrix profiles of the photocatalytic degradation of chlorophenols and phenol in continuous-flow reactors configured in series under suspended catalyst conditions. [TiO_2] 30 mg L^{-1}; Oxygen flow – 20 mL min^{-1}; Flow rate – 15 mL min^{-1}; [Analytes] ≈ 10 mg L^{-1}.

It is expected that the faster flow setting depicted in Figures 4 and 5 will experience lower PCP treatment performances. This is evident in that near complete treatment of PCP is achieved in the second reactor and third reactor using the 15 and 30 mL min^{-1} flow-rates respectively. Data in Table 3 shows that the oxidation of PCP strictly followed the unmodified Langmuir-Hinshelwood kinetics, and merged system calculations suggest that complete PCP oxidation takes approximately 30 minutes of radiation exposure. The performance matrices and calculations show that near complete TCP oxidation takes approximately 180 minutes across of the reactors applied. Singular compound performance profiles suggested that complete degradation of TCP took place in approximately 100 minutes of irradiation.

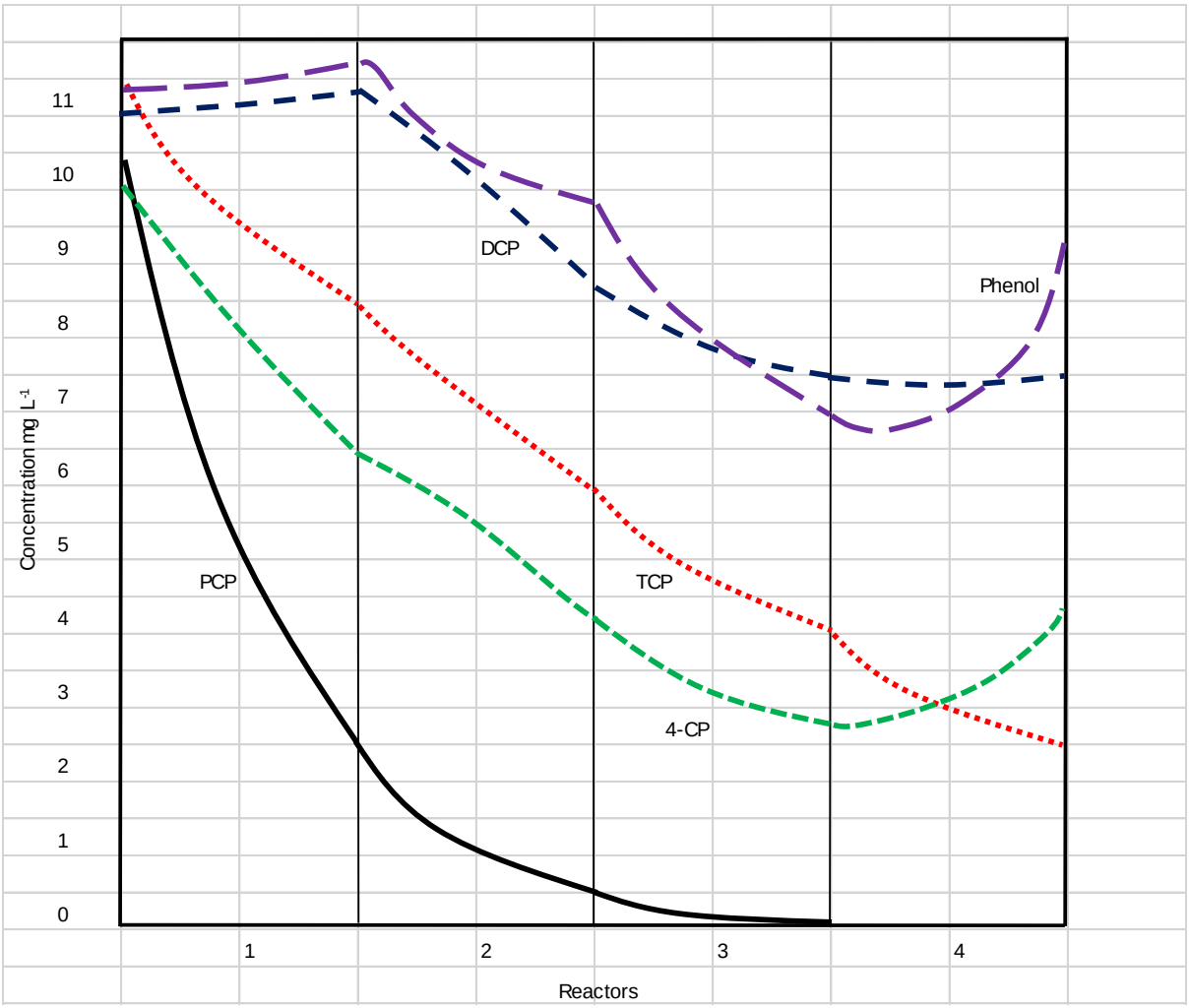

Figure 6 Performance matrix profiles of the photocatalytic degradation of chlorophenols and phenol in continuous-flow reactors configured in series under suspended catalyst conditions. [TiO_2] 30 mg L^{-1}; Oxygen flow – 20 mL min^{-1}; Flow rate – 30 mL min^{-1}; [Analytes] ≈ 10 mg L^{-1}.

Even without the assumption that compound to compound interactions and catalyst selectivity play roles, the detected concentrations of TCP and other lesser substituted chlorophenols suggest accumulative effects that are not directly plausible by strict L-H principles. The performance matrices show that there are fractional increases in TCP concentrations with the consumption of PCP. The 9 mL min^{-1} matrix shows that there is an increasing form of degradation of the profile that reaches its minimum upon complete disappearance of PCP. The 15 mL mim^{-1} matrix validates this by having recorded highest exponential increases in TCP when there was a significant increase in the removal of PCP. This marked increase was sharpened by the influence of available photon energy, the inner-placed reactor vessels are exposed to higher photon delivery than the outer-placed vessels.

Table 3 Estimated parameters of the photocatalytic transformations of chloride-substituted phenolics in suspended sets

Analyte	**PCP**		**TCP**				**DCP**				**4-CP**				**Phenol**			
	K	***k***	***K***	***k***	***k*₂**	***R***	***K***	***k***	***k*₂**	***R***	***K***	***k***	***k*₂**	***R***	***K***	***k***	***k*₂**	***R***
Flow-rate																		
8.8 mL min-1																		
Reactor																		
1	*0.03*	*3.058*	*0.069*	*0.002*	*0.0043*	*0.126*	*0.135*	*0.0550*	*0.1070*	*0.00087*	*0.073*	*0.0396*	*0.0119*	*0.0675*	*0.070*	*-0.058*	*0.0217*	*0.0730*
			0.070	*0.571*	*0.0356*	*0.083*												
2			*0.061*	*0.411*	*0.0235*	*0.011*	*0.128*	*0.1433*	*0.0878*	*0.0017*	*0.090*	*0.3586*	*0.0023*	*0.3761*	*0.0684*	*0.435*	*0.0115*	*0.0501*
															0.0502	*-0.406*	*0.0101*	*0.1654*
3			*0.054*	*0.785*	*0.0081*	*0.051*	*0.123*	*0.2830*	*0.0449*	*0.0055*	*0.090*	*0.2090*	*0.0183*	*0.0256*	*0.0501*	*-0.762*	*0.0098*	*0.1517*
4							*0.123*	*0.1646*	*0.0442*	*0.0055*	*0.067*	*0.0919*	*0.0076*	*0.0034*	*0.0456*	*0.0687*	*0.0422*	*0.00016*
Flow-rate																		
15 mL min-1																		
Reactor																		
1	*0.03*	*5.049*	*0.1070*	*0.526*	*0.1485*	*0.006*	*0.126*	*0.0372*	*0.0142*	*0.0476*	*0.082*	*0.5680*	*0.2199*	*0.0015*	*0.07*	*-0.042*	*0.0776*	*2.5E-5*
2			*0.1074*	*0.035*	*0.0573*	*0.020*	*0.144*	*-0.168*	*0.0114*	*0.0261*	*0.074*	*-0.097*	*0.0157*	*0.0015*	*0.0510*	*-0.269*	*0.0089*	*0.0223*
3			*0.0569*	*1.373*	*0.0491*	*0.066*	*0.145*	*0.2830*	*0.0191*	*0.1069*	*0.072*	*0.7028*	*0.1016*	*0.0103*	*0.0672*	*0.1735*	*0.0104*	*3.7E-5*
4			*0.0502*	*0.506*	*0.0023*	*0.090*	*0.143*	*0.0360*	*0.0163*	*0.0287*	*0.090*	*-0.139*	*0.0095*	*0.0082*	*0.0527*	*-0.115*	*0.0016*	*0.0015*
Flow-rate																		
30 mL min-1																		
Reactor																		
1	*0.03*	*4.515*	*0.05*	*0.867*	*0.3673*	*0.002*	*0.151*	*0.0287*	*0.0875*	*0.0152*	*0.075*	*0.8054*	*-*	*-*	*0.07*	*-0.052*	*0.3465*	*0.0010*
2	*0.03*	*5.869*	*0.05*	*1.165*	*0.2270*	*0.012*	*0.120*	*0.3758*	*-*	*-*	*0.077*	*0.2961*	*0.3014*	*0.0057*	*0.0623*	*0.559*	*0.2742*	*0.0084*
3			*0.0889*	*0.905*	*0.2847*	*0.008*	*0.121*	*0.3951*	*0.0605*	*0.1818*	*0.077*	*0.9672*	*0.1853*	*0.0225*	*0.0652*	*1.432*	*0.5891*	*0.0008*
4			*0.0985*	*1.011*	*0.3214*	*0.004*	*0.141*	*0.0874*	*0.1054*	*0.0364*	*0.051*	*-0.851*	*0.0575*	*0.0006*	*0.0500*	*-0.657*	*0.009*	*0.0007*

Table 4 Best fit exponential growth/decay model integrated into LH expression of the suspended catalyst

Analyte	TCP	DCP	4-CP	Phenol
Flow-rate				
9 mL min^{-1}				
Reactor				
1	$R_n.e^{kt}$/ $R_n.(1- e^{kt})$	$R_n.e^{kt}$	$R_n.e^{kt}$	$R_n.(1- e^{kt})$
2	$R_n.(1- e^{kt})$	$R_n.e^{kt}$	$R_n.(1- e^{kt})$	$R_n.(1- e^{kt})$
3	$R_n.(1- e^{kt})$	$R_n.(1- e^{kt})$	$R_n.(1- e^{kt})$	$R_n.e^{kt}$
4	-	$R_n.(1- e^{kt})$	$R_n.e^{kt}$	$R_n.e^{kt}$
Flow-rate				
15 mL min^{-1}				
Reactor				
1	$R_n.(1- e^{kt})$	$R_n.e^{kt}$	$R_n.(1- e^{kt})$	$R_n.e^{kt}$
2	$R_n.e^{kt}$	$R_n.e^{kt}$	$R_n.e^{kt}$	$R_n.e^{kt}$
3	$R_n.(1- e^{kt})$	$R_n.(1- e^{kt})$	$R_n.(1- e^{kt})$	$R_n.(1- e^{kt})$
4	$R_n.e^{kt}$	$R_n.e^{kt}$	$R_n.(1- e^{kt})$	$R_n.(1- e^{kt})$
Flow-rate				
30 mL min^{-1}				
Reactor				
1	$R_n.(1- e^{kt})$	$R_n.(1- e^{kt})$	$R_n.e^{kt}$	$R_n.(1- e^{kt})$
2	$R_n.e^{kt}$	$R_n.e^{kt}$	$R_n.e^{kt}$	$R_n.(1- e^{kt})$
3	$R_n.(1- e^{kt})$	$R_n.(1- e^{kt})$	$R_n.(1- e^{kt})$	$R_n.(1- e^{kt})$
4	$R_n.(1- e^{kt})$	$R_n.(1- e^{kt})$	$R_n.(1- e^{kt})$	$R_n.(1- e^{kt})$

Time based extrapolations of Figure 6 also show a supporting marked increase at almost the same period that was recorded irrespective of photon delivery. The observed behaviour of MCP in the early stages suggests that it has a higher propensity of adsorption under slurry catalyst conditions. In longer detention periods MCP's efficiency decreases and reforms the expected derivative profile, where its accumulative increase agrees with the subsequent oxidative contributions for higher level chlorinated phenols. DCP appears to initially follow the exponential growth degradation kinetics, an important assumption of Langmuir adsorption is that, a fixed number of vacant or adsorption sites are available on the solid catalyst surface. This means that if higher level substituted chlorophenols are preferentially adsorbed, DCP oxidation will be stagnant and accumulation of the subsequently formed DCP takes effect, this increase will be subjected to the presence or disappearance of TCP. The last two reactors recorded the highest rates of DCP degradation that took place as the amount of TCP in solution was almost completely diminished.

Phenol can be viewed as the stem compound substituted with chloride ions, the oxidation clipping of all the chloride ions results in phenol. As the most conformationally stable compound in solution, and the evidence in Figure 4 of the aggressive manner that MCP was degraded at this early stages, phenol is expected to be initially subject to a negative rate of degradation. The estimated parameters of the rate constants in Table 3, recorded values in agreement, there is a general increase in phenol concentration with progressive detention periods. In all determinations the irradiation periods were not sufficient at removing phenol to significant reduction levels. It can be speculated that maximum occupation of catalyst surface sites by higher substituted would leave lesser chlorohalogenated phenolics and phenol outcompeted. The degradation of phenol and the limitation of its oxidation are offset by the rate of accumulation resulting in negative rate of degradation.

Photocatalytic oxidation of chlorophenols in immobilised catalyst

Similar photocatalytic performance matrices were constructed for the immobilised photocatalyst experiments. These are viewed independently to the suspended slurry catalyst applications. The aim was to determine the impact of compromised photo delivery and mass transfer to the photodegradation of chlorophenols in the same reactor configuration. The secondary objective was to determine the effect of the photocatalytic degradation of organics on non-ideal support material such as glass, and probable justification of preliminary implementations of a non-optimised photocatalytic system to negate the catalyst particle reclamation problem, which has seen stagnation in this technological progress.

Due to the slurry nature of the suspended photocatalyst application and the size of the oxide particles, experimental solutions turn murky and translucent. This results in somewhat impaired photon delivery where the catalyst concentration is relatively dense, this however does not affect mass transfer. The photocatalyst immobilised applications improves the photon delivery aspect as particles are not suspended in solution and light can penetrate through a transparent liquid medium. However, the mass transfer aspect is limited due to lower numbers of available particle active sites, so one of either mass transfer or photon delivery in reactor design is improved at the expense of the other.

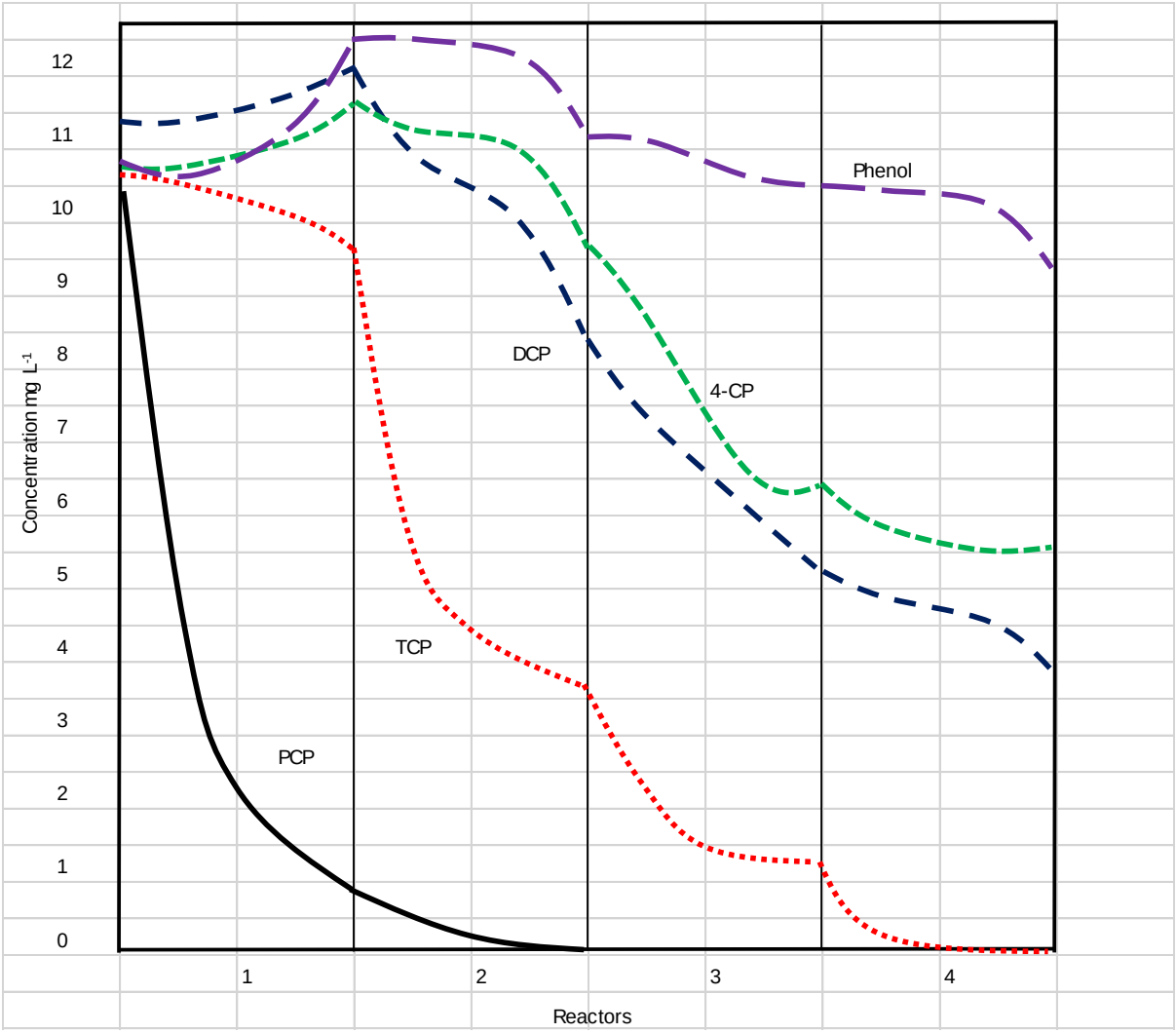

Figure 7 Performance matrix profiles of the photocatalytic degradation of chlorophenols and phenol in continuous-flow reactors configured in series under immobilised catalyst conditions. Oxygen flow – 20 mL min^{-1}; Flow rate – 9 mL min^{-1}; [Analytes] ≈ 10 mg L^{-1}.

In this project, the configured immobilised system experiences both mass transfer limitations resulting from the immobilised format of catalyst application and photon delivery impairment due to reduced photon transmittance though the thin layer oxide film, and light scattering due to optical hindrance. The performance of the immobilised set provides a feasibility assessment of the potential positive application of the technology in its raw state versus the limitations. Though equivalent solution flow-rates were replicated, the reactor vessel detention periods are different due to packing-displaced volume and therefore totally different oxidation kinetics are expected, so direct comparison to suspended catalyst performance matrices is implausible. The impressions of a compromised system from both the mass transfer and photon delivery can be judged strictly from a photocatalytic efficiency stand-point.

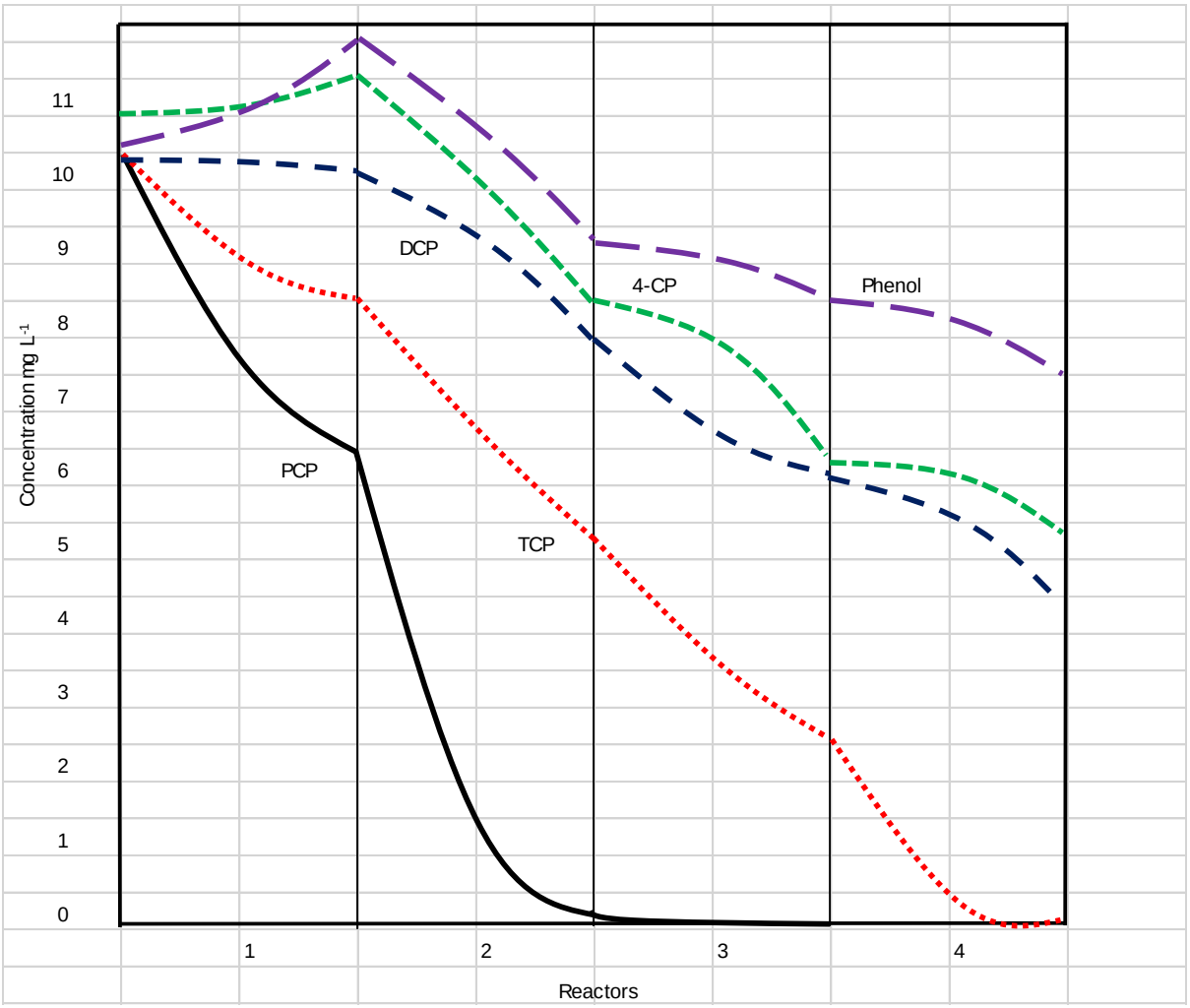

Figure 8 Performance matrix profiles of the photocatalytic degradation of chlorophenols and phenol in continuous-flow reactors configured in series under immobilised catalyst conditions. Oxygen flow – 20 mL min^{-1}; Flow rate – 15 mL min^{-1}; [Analytes] ≈ 10 mg L^{-1}.

The network packed reactors measured average volumes of 230 ± 5 mL, which was approximately over 42 percent of reduction in solution volume, therefore a totally independence system was investigated. It was also important to determine the impact of the glass packing without catalyst film as a means of a control set, photolysis contribution was the control and the limitations associated with it packed material. A paper in IPCBEE (2015) that was conducted on the batch systems of a similar investigation performed control studies, including the photolytic efficiency of the glass packing in the absence of the immobilised photocatalyst. The results of that study showed that less than 30 percent of the starting concentrations of most compounds were degraded in the uncoated film sets against the catalyst immobilised sets after a period of over 180 minutes.

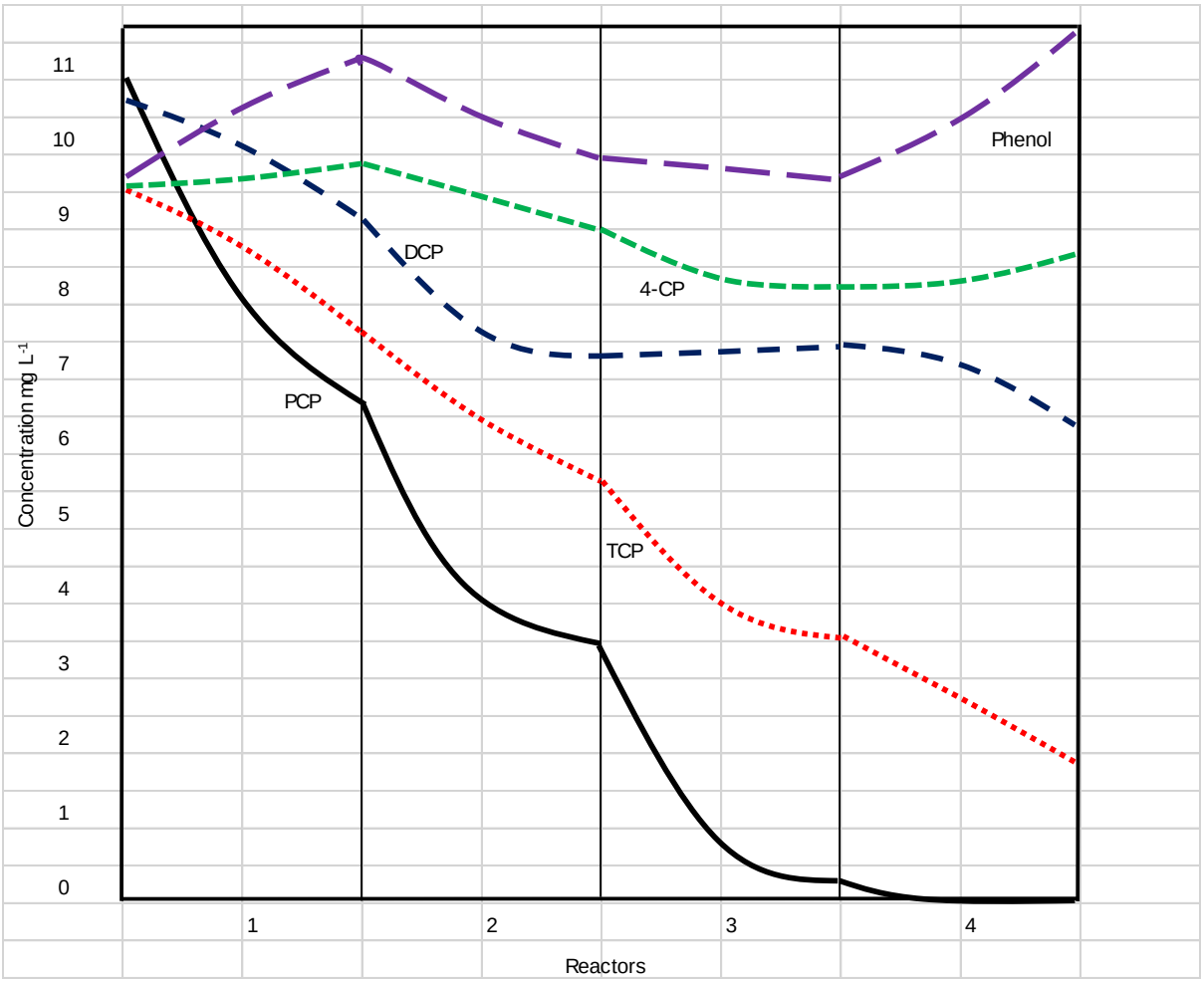

Figure 9 Performance matrix profiles of the photocatalytic degradation of chlorophenols and phenol in continuous-flow reactors configured in series under immobilised catalyst conditions. Oxygen flow – 20 mL min^{-1}; Flow rate – 30 mL min^{-1}; [Analytes] ≈ 10 mg L^{-1}.

Where near 100 percent of compound degradation was achieved in the catalyst sets. It can be extrapolated and assumed that the photocatalytic process has significantly improved efficiency versus photolysis even under the current project conditions. The performance matrix in Figure 7 shows a similar compound removal sequence to that of suspended sets. The expected difference would be in the treatment efficiency of each compound, under conditions where reaction drivers are limited and the source pollutants are of a significantly low volume. What is evident in all the immobilised performance matrix sets is that there is a steadier nature of chemical transformation in the fractional dehalogenation of most starting chlorophenol compounds, especially the higher substituted species.

Table 5 Estimated parameters of the photocatalytic transformations of chloride-substituted phenolics in immobilised sets

Analyte	**PCP**		**TCP**				**DCP**				**4-CP**				**Phenol**			
	K	***k***	***K***	***k***	***k*₂**	***R***	***K***	***k***	***k*₂**	***R***	***K***	***k***	***k*₂**	***R***	***K***	***k***	***k*₂**	***R***
Flow-rate																		
8.8 mL min-1																		
Reactor																		
1	*0.0308*	*3.292*	*0.104*	*-0.02*	*0.0079*	*0.040*	*0.159*	*-0.012*	*0.0086*	*0.132*	*0.090*	*0.0010*	*0.0621*	*0.0177*	*0.0592*	*0.0835*	*0.0352*	*0.112*
2			*0.053*	*1.546*	*0.039*	*0.140*	*0.159*	*-0.034*	*0.0099*	*0.118*	*0.077*	*-0.085*	*0.0402*	*0.0531*	*0.0516*	*-0.294*	*0.0156*	*0.114*
3			*0.055*	*1.352*	*0.0086*	*0.177*	*0.159*	*0.2449*	*0.0062*	*0.129*	*0.082*	*-0.127*	*0.0709*	*0.0935*	*0.0550*	*0.0834*	*0.0261*	*0.124*
											0.085	*0.7511*	*0.0746*	*0.1085*	*0.0557*	*0.210*	*0.0158*	*0.239*
4							*0.123*	*-0.294*	*0.0057*	*0.133*	*0.055*	*-0.117*	*0.0047*	*0.0629*	*0.0574*	*-0.589*	*0.0105*	*0.198*
Flow-rate																		
15 mL min-1																		
Reactor																		
1	*0.03*	*1.249*	*0.088*	*0.314*	*0.0220*	*0.114*	*0.155*	*-0.025*	*0.0132*	*0.0207*	*0.050*	*-0.035*	*0.381*	*0.0002*	*0.0500*	*0.0447*	*0.0405*	*0.2066*
2	*0.0575*	*3.917*	*0.087*	*0.037*	*0.0398*	*0.124*	*0.157*	*-0.261*	*0.0301*	*0.213*	*0.051*	*0.164*	*0.0479*	*0.0828*	*0.0500*	*-0.944*	*0.0168*	*0.4167*
3			*0.059*	*0.484*	*0.0052*	*0.066*	*0.124*	*0.327*	*0.0801*	*0.299*	*0.051*	*-0.309*	*0.0593*	*0.1048*	*0.0500*	*-1.503*	*0.0042*	*0.4754*
4			*0.058*	*<lmt*	*0.0027*	*0.050*	*0.126*	*0.043*	*0.1274*	*0.0248*	*0.052*	*-0.208*	*0.0327*	*0.1003*	*0.0500*	*-1.625*	*0.0084*	*0.4777*
Flow-rate																		
28 mL min-1																		
Reactor																		
1	*0.03*	*2.623*	*0.1098*	*0.187*	*0.7260*	*0.001*	*0.160*	*-1.49*	*0.0186*	*0.999*	*0.052*	*-0.093*	*0.794*	*0.0002*	*0.07*	*-0.355*	*-*	*-*
2	*0.03*	*0.397*	*0.0604*	*0.792*	*0.0325*	*0.044*	*0.158*	*0.573*	*0.4354*	*0.0096*	*0.051*	*0.5211*	*0.843*	*0.0001*	*0.07*	*0.251*	*0.0068*	*0.0022*
3	*0.0320*	*<lmt*	*0.0522*	*1.566*	*0.0001*	*0.001*	*0.148*	*-0.012*	*0.2834*	*0.0032*	*0.051*	*0.5243*	*0.879*	*0.0001*	*0.0699*	*0.142*	*0.0069*	*0.0057*
4			*0.0530*	*-0.67*	*0.0465*	*0.201*	*0.154*	*-0.138*	*0.1353*	*0.0930*	*0.052*	*-0.067*	*0.908*	*0.0001*	*0.050*	*-0.222*	*0.0304*	*<1*

Table 6 Best fit exponential growth/decay model integrated into LH expression of the immobilised catalyst

Analyte	**TCP**	**DCP**	**4-CP**	**Phenol**
Flow-rate				
8.8 mL min^{-1}				
Reactor				
1	$R_n.e^{kt}$	$R_n.(1- e^{kt})$	$R_n.(1- e^{kt})$	$R_n.(1- e^{kt})$
2	$R_n.(1- e^{kt})$	$R_n.e^{kt}$	$R_n.e^{kt}$	$R_n.e^{kt}$
3	$R_n.(1- e^{kt})$	$R_n.(1- e^{kt})$	$R_n.e^{kt}$ /$R_n.(1- e^{kt})$	$R_n.e^{kt}$/ $R_n.(1- e^{kt})$
4	-	$R_n.e^{kt}$	$R_n.e^{kt}$	$R_n.e^{kt}$
Flow-rate				
15 mL min^{-1}				
Reactor				
1	$R_n.(1- e^{kt})$	$R_n.e^{kt}$	$R_n.(1- e^{kt})$	$R_n.(1- e^{kt})$
2	$R_n.e^{kt}$	$R_n.e^{kt}$	$R_n.e^{kt}$	$R_n.e^{kt}$
3	$R_n.e^{kt}$	$R_n.(1- e^{kt})$	$R_n.e^{kt}$	$R_n.e^{kt}$
4	$R_n.(1- e^{kt})R_n.e^{kt}$	$R_n.e^{kt}$	$R_n.e^{kt}$	$R_n.e^{kt}$
Flow-rate				
28 mL min^{-1}				
Reactor				
1	$R_n.e^{kt}$	$R_n.e^{kt}$	$R_n.(1- e^{kt})$	$R_n.(1- e^{kt})$
2	$R_n.(1- e^{kt})$	$R_n.(1- e^{kt})$	$R_n.(1- e^{kt})$	$R_n.e^{kt}$
3	$R_n.e^{kt}$	$R_n.(1- e^{kt})$	$R_n.(1- e^{kt})$	$R_n.(1- e^{kt})$
4	$R_n.e^{kt}$	$R_n.e^{kt}$	$R_n.(1- e^{kt})$	$R_n.(1- e^{kt})$

The lower substituted phenolics depict erratic type transformations especially later in the treatment process, this may be related to the compounds relatedness and the higher degree photocatalytic activities in the absence of the selectively preferred higher level chlorosubstituted phenols. Table 5 recorded fractional conversion coefficients for the immobilised sets that appear to be higher than those of the suspended catalyst sets, this may be explained by the nature of photon delivery and mass transfer limitations, where the inefficiency in performance slows the transformation protocol resulting in the subsequently formed derivatives to exist in the system just a bit that longer before subjected to oxidation. The performance profile matrices of the packed network systems are evidence to suggest that treatment of organic micro-pollutants using non optimized systems can be viable applications.

Conclusion

The study focus was on experimental intricacies of heterogeneous semiconductor photocatalysis in the oxidation and treatment of polychlorinated substituted phenolic compounds as a representative class of chemicals. The objective was to determine chemical transformation kinetics of multiple pollutant representative compounds that are simultaneously treated using photocatalytic advanced oxidation technology in aqueous systems. The photocatalytic mechanism is a complex one, though the theoretical concept is understood, the reaction schemes that are responsible for the products are still unclear. The chemical transformations of simultaneously photocatalysed polychlorinated substituted phenols are fractionally accumulative at the expense of others, which mean that the consumption of higher level substituted chlorophenols led to an increase in the concentrations of lower level substituted chlorophenols. The Langmuir-Hinshelwood expression required modification to incorporate population growth dynamics that could explain this behaviour. It was found that there was merit in the immobilization of the photocatalyst onto a non-ideal material as a preliminary application of the technology.

Acknowledgement

Funding from the Water Research Commission (WRC) of South Africa through the WRC Project No. K5/1125//3 awarded to Prof Evans M.N. Chirwa of the University of Pretoria.

Symbols

C	Concentration of analyte	mg L^{-1}
C_e	Equilibrium solution concentration	mg L^{-1}
K	Adsorption constant	mg L^{-1}
k	Oxidation constant	mg L^{-1} min^{-1}
K_L	Langmuir adsorption constant	mg L^{-1}
K_{2n}	Accumulative transformation constant	mg L^{-1} min^{-1}

Q_e Adsorbed chemical concentration mg g^{-1}

Q_m Maximum adsorption capacity mg g^{-1}

r Rate of degradation mg L^{-1} min^{-1}

R_n Fractional conversion coefficient

References

Ângelo J., Andrade L., Madeira L. M. and Mendes A. (2013). An overview of photocatalysis phenomena applied to NOx abatement. *J Environ Manage.* **129**(0), 522-539.

Carp O., Huisman C. L. and Reller A. (2004). Photoinduced reactivity of titanium dioxide. *Progress in Solid State Chemistry.* **32**(1–2), 33-177.

Chen D., Sivakumar M. and Ray A. K. (2000). Heterogeneous photocatalysis in environmental remediation. *Dev Chem Eng Miner Process.* **8**(5-6), 505-550.

Davis A. P., Huang C. P. (1990). The removal of substituted phenols by a photocatalytic oxidation process with cadmium sulfide. *Water Res.* **24**(5), 543-550.

Demeestere K., Dewulf J. and Van Langenhove H. (2007). Heterogeneous Photocatalysis as an Advanced Oxidation Process for the Abatement of Chlorinated, Monocyclic Aromatic and Sulfurous Volatile Organic Compounds in Air: State of the Art. *Crit Rev Environ Sci Technol.* **37**(6), 489-538.

Khuzwayo Z., Chirwa E. M. N. (2015b). Analysis of Recycled-Glass Immobilised and Suspended TiO_2 in the Photocatalytic Oxidation of Chlorophenols in Batch Processes. *IPCBEE.* **90**, 121-126.

Khuzwayo Z., Chirwa E. M. N. (2015a). Modelling and simulation of photocatalytic oxidation mechanism of chlorohalogenated substituted phenols in batch systems: Langmuir–Hinshelwood approach. *J Hazard Mater.* **300**, 459-466.

Kumar K. V., Porkodi K. and Rocha F. (2008). Langmuir–Hinshelwood kinetics – A theoretical study. *Catalysis Communications.* **9**(1), 82-84.

Lathasree S., Rao A. N., SivaSankar B., Sadasivam V. and Rengaraj K. (2004). Heterogeneous photocatalytic mineralisation of phenols in aqueous solutions. *Journal of Molecular Catalysis A: Chemical.* **223**(1–2), 101-105.

Malato S., Fernández-Ibáñez P., Maldonado M. I., Blanco J. and Gernjak W. (2009). Decontamination and disinfection of water by solar photocatalysis: Recent overview and trends. *Catalysis Today.* **147**(1), 1-59.

Metcalf E. I. (2003). **Wastewater engineering** : treatment and reuse. McGraw-Hill, Boston : London.

Nugraha J., Fatimah I. (2013). Evaluation of photodegradation efficiency on semiconductor immobilized clay photocatalyst by using probit model approximation. *International Journal of Chemical and Analytical Science.* **4**(2), 125-130.

Oller I., Malato S. and Sanchez-Perez J. A. (2011). Combination of advanced oxidation proceses and biological treatemnt for wastewater decontamination. A review. *Science of The Total Environment.* **409**(20), 4141-4166.

Pelentridou K., Stathatos E., Karasali P. and Lianos P. (2009). Photodegradation of the herbicide azimsulfuron using nanocrystalline titania films as photocatalyst and low intensity Black Light radiation or simulated solar radiation as excitation source. *Journal of hazardous materials.* **163**, 756-760.

Pera-Titus M., García-Molina V., Banos M. A., Giménez J. and Esplugas S. (2004). Degradation of chlorophenols by means of advanced oxidation processes: a general review. *Applied Catalysis B: Environmental.* **47**, 219-256.

Pozzo R. L., Baltanás M. A. and Cassano A. E. (1997). Supported titanium oxide as photocatalyst in water decontamination: State of the art. *Catalysis Today.* **39**(3), 219-231.

Saien J., Khezrianjoo S. (2008). Degradation of the fungicide carbendazim in aqueous solutions with UV/TiO2 process: Optimization, kinetics and toxicity studies. *J Hazard Mater.* **157**(2–3), 269-276.

Yasmina M., Mourad K., Mohammed S. H. and Khaoula C. (2014). Treatment Heterogeneous Photocatalysis; Factors Influencing